# Investigation of the Measurability of Selected Damage to Supporting Structures of Wind Turbines

**J Rupfle[1], A Emiroglu[2], C U Grosse[1]**

[1] Chair of Non-destructive Testing, Technical University of Munich, Franz-Langinger-Str. 10, 81245 Munich

[2] Chair of Structural Analysis, Technical University of Munich, Arcisstr. 21, 80333 Munich

E-mail: johannes.rupfle@tum.de, grosse@tum.de

**Abstract.** The present work deals with a measurability study of damage to supporting structures of wind turbines. The examined hybrid tower consists of a prestressed concrete part with an attached steel section on top. Principal focus is on developing a data preprocessing and analysis concept aiming to investigate the measurability of the two selected failure cases *missing pretension of tendons* and *fatigue based change of Young's modulus in reinforcement concrete*. A simulation deduced out of real world mass and thrust forces provides a comparison with measured data based tower displacements, natural frequencies and mode shapes. The measurability of given deviations is investigated by means of virtual sensors, derived from the measurement setup of a test facility measuring acceleration, velocity, displacement and strain on different positions of the wind turbine tower, aiming the development of detection methods of such cases of damage for condition monitoring systems. The simulation input can be given by strain-based external forces or vibration-based displacements.

## 1. Introduction

Condition Monitoring has established itself in the past years as an instrument for damage detection. The project *IM Wind* as well as the previous project *MISTRALWIND* are focused on long-term monitoring of wind turbines [1]. The present work is concerned with measurement techniques for the detection of damage to the supporting structures of wind turbines. Using a construction plan and statics based model, the measurability of missing pretension of tendons and fatigue based change of Young's modulus in reinforcement concrete as failure cases influencing Eigenfrequencies, damping values and mode shapes is discussed.

A comprehensive literature research and reflected discussions with experts led to a number of possible damages to supporting structures of wind turbines. An overview of all considered damages is given in figure 1. In case of the within the framework of the project equipped hybrid tower, damage is mainly concentrated on connecting elements [2] [3]. A group of experts around the IM Wind Project carried out a final selection of the damage cases to be considered in the evaluation.

As the hybrid tower consists of a prestressed concrete part, tendons are used to avoid stress in reinforcement concrete to avoid damage. The pretensioning force is adjusted with a hydraulic

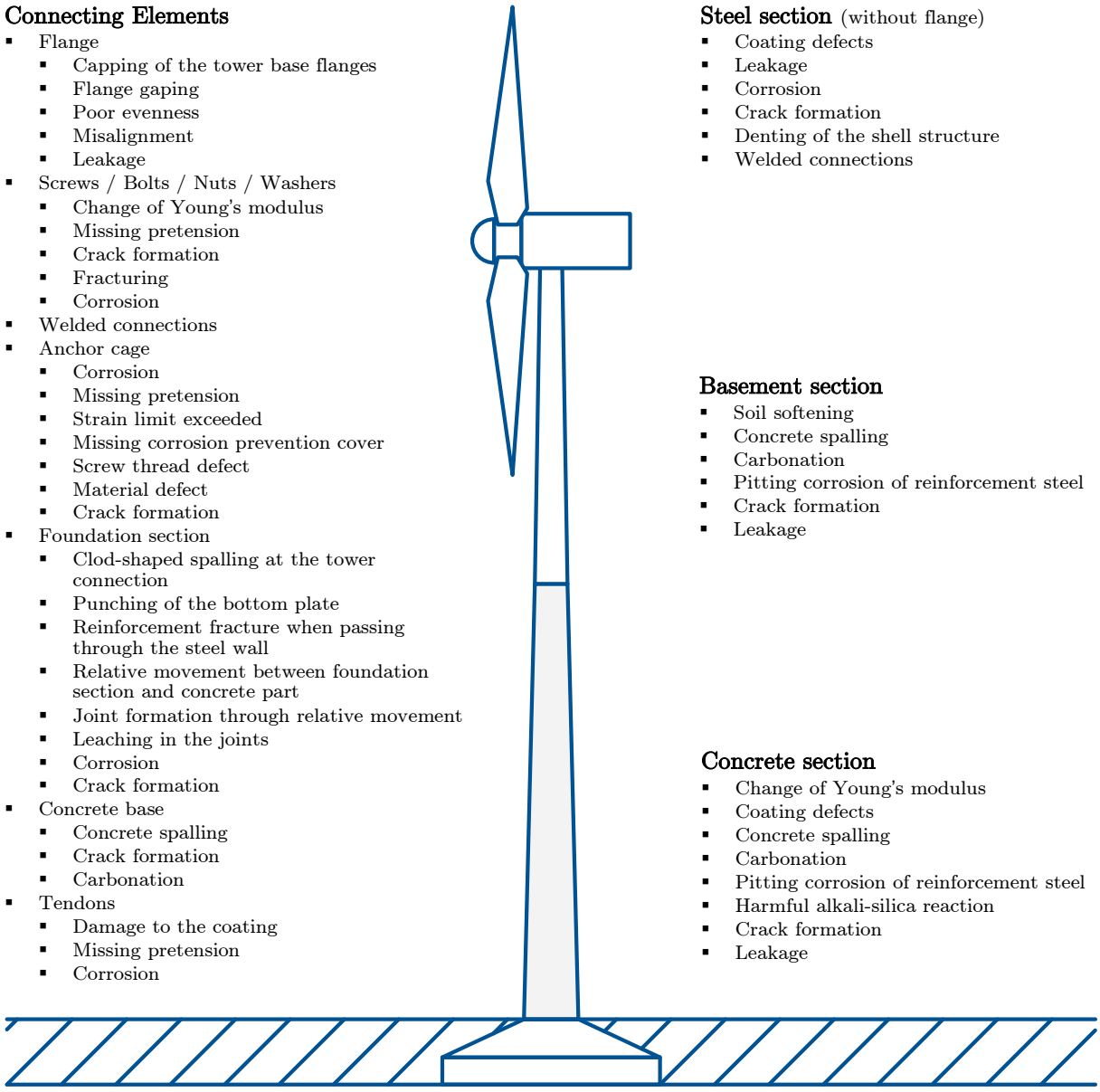


**Figure 1.** Possible damage considered in the evaluation process divided into subsections.

press and must be checked at regular intervals. Since a missing prestressing force will have a direct effect on the overall stiffness of the tower, it can be assumed that this can be recorded by measuring techniques.

Furthermore, degradation of reinforced concrete is investigated. As examined by Musiał [4] and Owen [5], the Young's modulus of reinforced concrete can be determined by measuring the Eigenfrequencies. Vibrational data can be used to monitor small changes in stiffness of reinforced concrete associated with slow degradation under cyclic load.

To gain knowledge about the measurability of damage in form of a reduced prestressing force, acceleration measurements of an equipped wind turbine are compared to simulation data based on mass and thrust forces derived from strain measurements combined with Supervisory Control and Data Acquisition (SCADA) data.

An essential element of the presented data preprocessing procedure is the Untwisting Cable Event (UCE) of a wind turbine. In this event, the twisted cable bundle in the tower of the turbine is untwisted to prevent damage. This specific condition is used to calibrate and synchronize measurement equipment.

## 2. Measurement Setup

The test facility is equipped with a variety of different measurement instruments to allow testing and validation of various approaches to a condition monitoring system and to investigate their accuracy. The sensors are distributed over five levels from the foundation up to the top of nacelle. All sensor axes are converted to a tower-fixed cylindrical coordinate system $x$-$y$-$z$ by means of composed elemental rotations with an intrinsic sequence $X$-$Y'$-$Z''$.

The main concept of the condition monitoring system is based on acceleration measurements, distributed over a height from 0 $m$ to 139 $m$. They are complemented by strain gauges at heights of 81 $m$ and 139 $m$, which are paired with temperature sensors. In addition to the strain gauges, a fiber optic measurement system with a total of eleven distributed strain and temperature sensors is located in the tower base area. A further seismometer is also located in the tower base. Tilt sensors are installed in the tower base and at a height of 139 $m$. In addition, a Real Time Kinetic (RTK) module is located on top of the nacelle, which provides a maximum resolution in the centimeter range and data with a sampling rate of 14 Hz. As the MISTRALWIND project shows, the Eigenfrequencies of the tower as well as from the rotor blades and influences of the rotor speed can be determined using measured data and used for further analysis [6]. The investigation of Botz et al. shows stabilization diagrams of different states of the turbine during a maintenance event. Stable poles are identified and their deviation during the maintenance event are analyzed. The setup is used for long-term monitoring of the structure and serves many research groups as a data basis for their investigations.

To better understand the movements of the tower, it is useful to be able to specify the displacement over the tower height. This cannot be precisely achieved based on acceleration measurements alone, since the double integration of the measured data represents an initial value problem and offset leads to accumulation of integration error. Values of the unknown function at a given point in the domain can be made available by additional sensors. For future research, RTK module on top of the nacelle can be used to provide an estimation of the displacement of nacelle and can be supplemented by a tilt sensor located near the upper acceleration sensor at 139 $m$. Knowing the displacement and inclination, the accelerometer can be complemented precisely at this point. Figure 2 illustrates the first four bending mode shapes of the tower, that can be observed using accelerometers. The first bending mode can be determined by one single accelerometer as there is an antinode located at the top of the tower. The second, third and fourth bending modes have nodes around the top location of the tower which makes it difficult to detect them with a single sensor.

## 3. Data Processing

In order to assess the measurability of damage, it is required to carry out an analysis with a real world load spectrum. Main focus of this section is on the challenges associated with the derivation of a load spectrum and the methods used to address them. A general workflow is developed that allows for data-driven simulation of damage cases. An approach is presented that separates the tower displacement calculation into three distinct components. The basic approach is the calculation of dynamic tower displacement using vibrational data. The application of ultra low frequency vibrational sensors with an ultra low noise density of 0.7 µg/Hz to 1.2 µg/Hz enables the determination of even lower frequency measurements up to the first bending

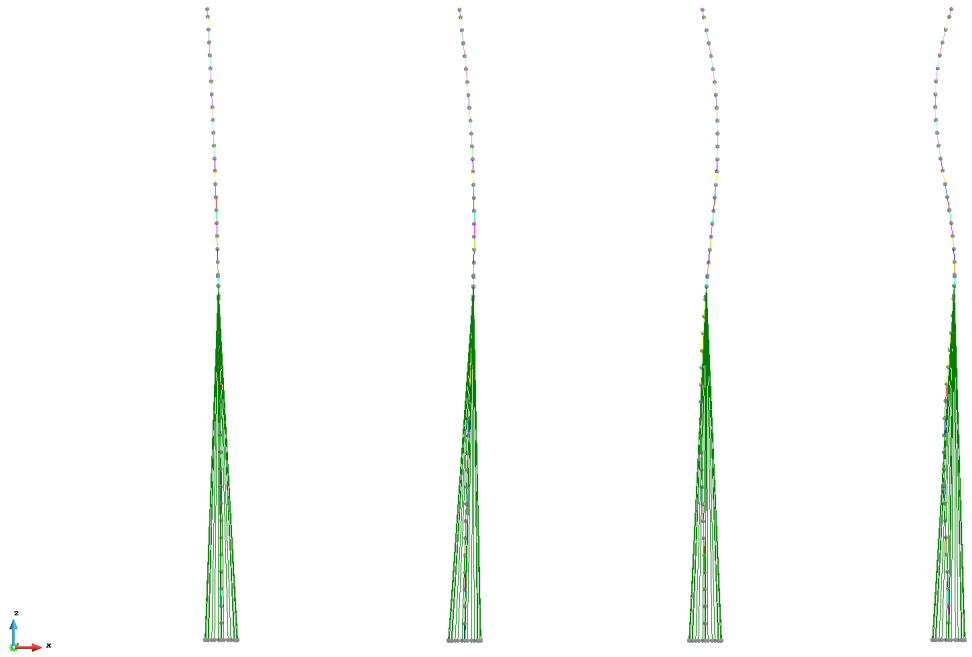

**Figure 2.** First four bending mode shapes of the tower finite element model.

eigenfrequency at around 0.27 Hz and a further combined natural frequency around 0.23 Hz. Furthermore, the static displacement of the tower, separated into mass induced and thrust force based displacement, is obtained from processed strain measurement data.

Figure 3 depitcs the seperation of static and dynamic displacements at 0.1 Hz which is below all known Eigenfrequencies of this specific wind turbine. To the extent known, below the first natural bending frequency of the tower, only resulting eigenmodes are found, which originate from the rotor speed in operation [6]. As the speed range lies within 7 RPM to 14 RPM, corresponding natural frequencies vary within a range of 0.11 Hz and 0.23 Hz.

In the present research work, the calculation of forces and displacement is based entirely on acceleration and strain measurements and is dealt with in section 3.3 and 3.4. An additional improvement through sensor data fusion is part of future research. An overview of possible combinations is given in section 3.5.

Furthermore, this section covers the required data pre-processing in form of measurement system synchronization in 3.1 and measurement based sensor calibration in 3.2.

### *3.1. Synchronization*

Synchronization of datasets from different sources is an important task for further analysis. Centralized, real-time data gathering with a unique timestamp is always strongly recommended. Application Programming Interfaces (API) of state-of-the-art measurement systems provide for real time data exchange at extremely high sampling rates. If no direct communication is possible, data must be synchronized using alternative techniques. Network Time Protocol (NTP) synchronization is a wide spread and robust method. A further improvement with accuracies up to sub-microsecond range [7] and minimal network and local clock computing resources is the use of Precise Time Protocol (PTP). Independently operating systems require alternative methods such as corresponding measurement signals.

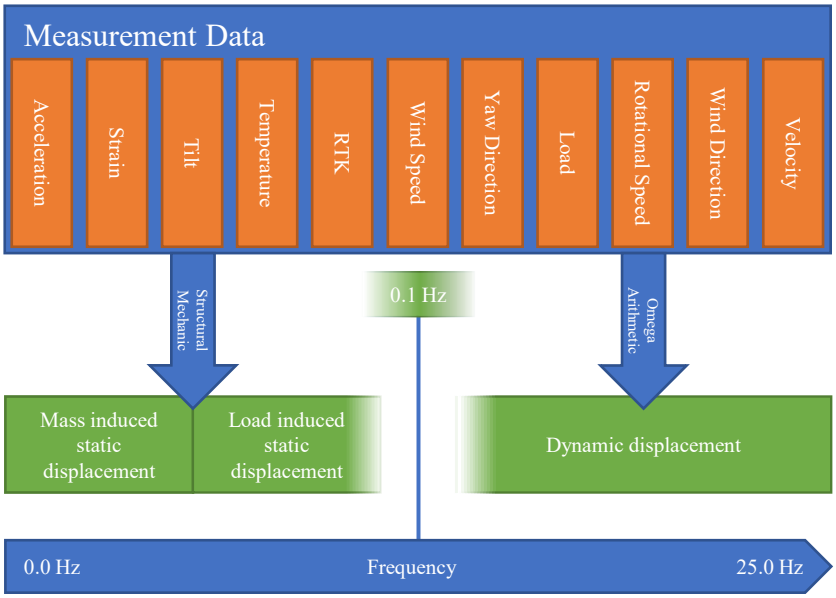


**Figure 3.** Data processing workflow

Due to the just recently established data interface between SCADA system and the edge controller, historical data requires alternative synchronization, since the timestamps diverge significantly at some points.

Using UCEs with their high repeatability results in precisions ranging up to milliseconds, depending on all other influencing factors. The yaw system of the test facility consists of eight electric gear motors that induce high momentum to supporting structures that further induces high shear stress to the tower due to the large mass moment of intertia of the rotor. Analysis of measurement signals revealed, that shear strain sensors detect a unique pattern of yaw drives starting up. SCADA status messages indicate the exact start of a UCE and are therefore suitable for pattern recognition. A representative pattern, extracted from measurement data is used for recognition using cross-correlation. Due to a duration of the UCE of more than 660 seconds, the extracted pattern is 320 seconds long to ensure viability and precision of detection of start of nacelle movement.

Figure 4 (a) describes yaw direction during an UCE and expected position of extracted and pre-processed shear strain pattern at the beginning of nacelle movement. All strain data are filtered with a high pass filter with a cutoff frequency of 0.1 Hz. Figure 4 (b) shows the acutal position of nacelle movement start in measurement data indicated with a black vertical line. Figure 4 (c) illustrates the aligned position of shear strain pattern due to normalized cross-correlation function shown in figure 4 (d).

### *3.2. Measurement based sensor calibration and position determination*

Because measurement accuracy is highly dependent on the sensor calibration, it is important to ensure proper calibration. A calibration certificate typically specifies sensitivity, frequency response, and offset of a sensor. This section demonstrates, as an example, the measurement-based recalibration of strain sensors using an UCE. The combined rotor and nacelle mass causes a static moment on the tower due to its center of gravity, resulting in strain that rotates with the nacelle position. During a UCE, the pitch angle is approximately 90°, allowing the assumption that the thrust force is low. If this is completely neglected because the wind speed is very low,

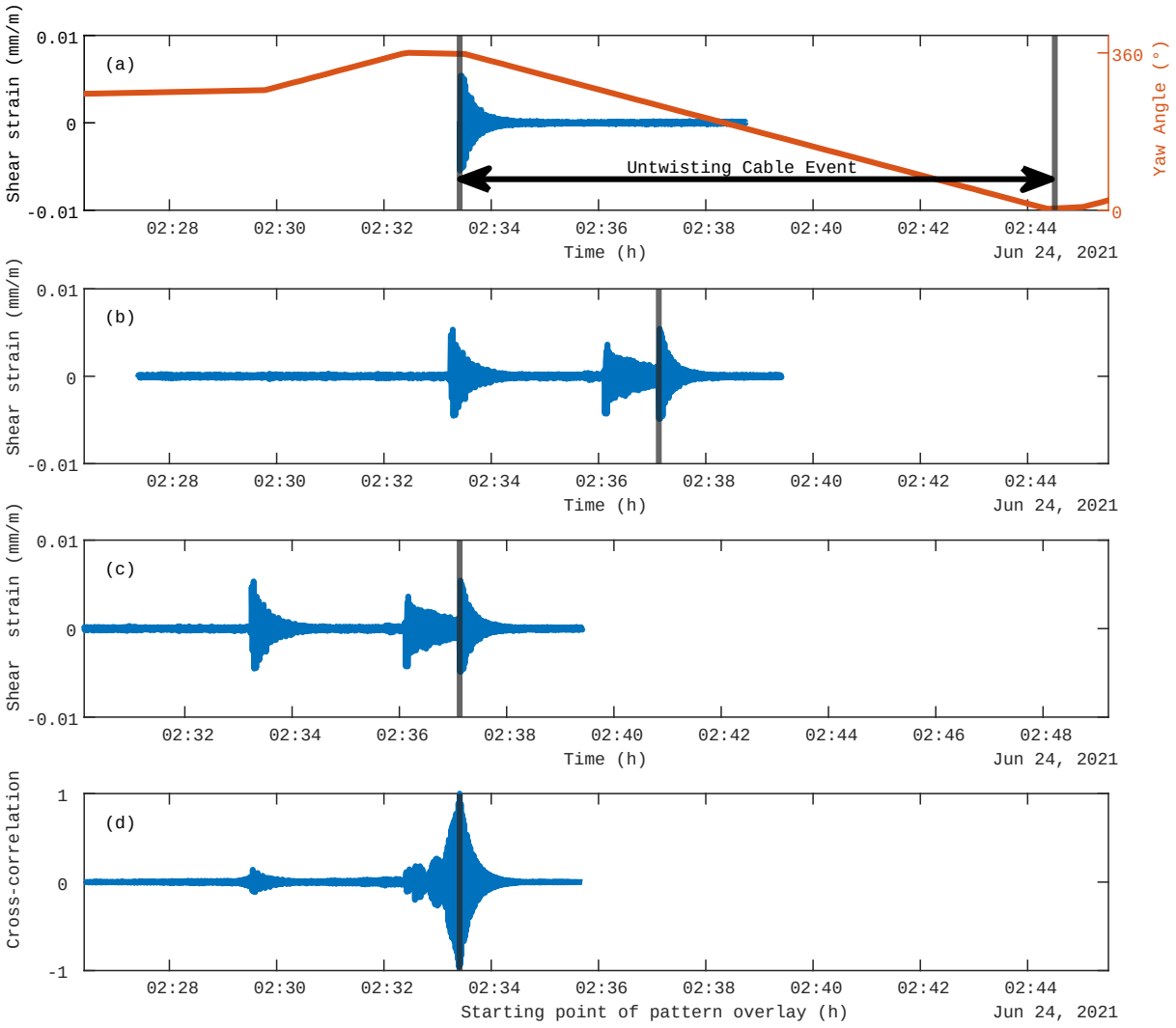


**Figure 4.** Data synchronization method using shear strain pattern recognition.
(a) Isolated and processed representative shear strain pattern of untwisting cable event (blue) and yaw angle (orange). Arrow indicates duration of UCE.
(b) Highpass filtered shear strain measurement. Horizontal line indicates start of UCE.
(c) Aligned shear strain measurement. Horizontal line indicates start of UCE.
(d) Normalized cross correlation of measurement data and representative pattern.

only static inertia forces impact the tower. The strain profile of a sensor is then represented by a sinusoidal function of the form represented by equation 1. The parameter indicate amplitude ($a = \frac{\epsilon_{max} - \epsilon_{min}}{2}$), period ($b = 1$, as period is equal to $2\pi$), strain gauge position as phase ($c = \alpha$, related to a clockwise rotation from true north in radians) and strain offset ($d = \frac{\epsilon_{max} + \epsilon_{min}}{2}$).

$$f(\theta, a, b, c, d) = a * cos(b * \theta + c) + d \tag{1}$$

Applying curve fitting by means of sum of squared residuals ($S$) as given in equation 2, leads to strain data during an UCE and thus to parameters $a$ to $d$ by minimizing $S$ as the residual is given by $r_i = f(t) - f(\theta, a, b, c, d)$. Optimization is then performed using a derivative-

free optimization algorithm. Figure 5 shows optimized model to an unprocessed real data set. Accuracy satisfies tolerance on function value of $1e^{-6}$.

The applied method can also be used to determine sensitivity, offset and position of accelerometers and tilt sensors as combined rotor and nacelle mass has a great influence on their horizontal axes as the influence of gravity is given by $sin(\alpha) * g$.

$$S = \sum_{i=1}^{n} (\epsilon(t) - f(\theta, a, b, c, d))_i^2 \tag{2}$$

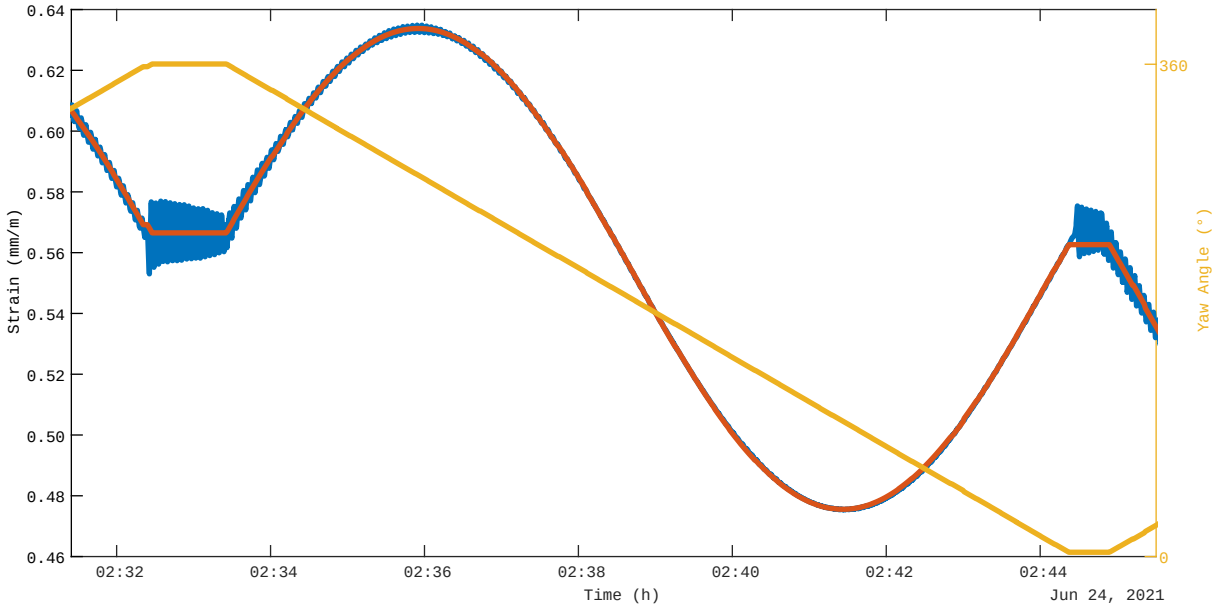


**Figure 5.** Comparison of unprocessed strain measurement (blue), optimized normal strain model (orange) with parameters $a = 0.079$, $b = 1.000$, $c = 81.053$ and $d = 0.555$ and yaw direction (yellow) during UCE.

### *3.3. Force calculation*

Static forces ($< 0.1$ Hz) are calculated using strain measurements. The strain is considered separately as the strain due to mass and the strain due to the thrust of the wind turbine. The first can be modeled using the parameterized model from equation 1. Subtracting mass induced strain from measured strain values leads to thrust based strain values. Both static strain components are then used to pure bending moment as $M_b = E * \epsilon_R * S$, where $E$, $\epsilon_R$ and S are Young's modulus, strain and section modulus. Forces are calculated according to $F = \frac{M_b}{h}$, where $h$ represents the distance of strain gauges from hub height.

### *3.4. Dynamic displacement calculation*

Calculation of displacement through acceleration data can be performed time discrete using a cumulative trapezoidal numerical integration or can be performed as frequency domain integration. In terms of real and noisy data, integration in frequency domain tends to be the more precise and reliable way of calculating displacement from acceleration measurement in practical application as stated in [8]. Direct integration in time domain causes drifts due to

offset in acceleration or random noise. A method to overcome this issue is proposed by Yang [9] and estimates a mean of upper and lower envelope to correct data.

The present investigation focuses on integration in frequency domain. A general workflow of the application of omega arithmetic, as this method is also referred to, is described in [10]. The practical implementation of the algorithm is inspired by [11].

For the present data set, the frequency range between 0.1 Hz and 25 Hz is considered. Filter parameter of high pass filter to eliminate DC components are set to a stop band frequency of 0.1 Hz and a stop band attenuation of 80 dB. Moreover, a tapered cosine window with a coverage of 4 % of data set is applied.

### *3.5. Uncertainty quantification*

In addition to the systematic and random errors that always appear, the measurements and analysis are subject to specific inaccuracies.

Synchronization of measurement data with SCADA data strongly depends on resolution of the yaw angle. Typically, SCADA data is not subject to a fixed cycle rate, but is event-triggered. As a result, the value is refreshed in response to a specified absolute or relative value change. With respect to synchronization, linear interpolation leads to unacceptable interpolation uncertainty. An interpolation scheme using previous values significantly reduces the error. Taking advantage of the fact that the yaw drives operate at a fixed speed, an advanced interpolation method can be applied. By determining the angular velocity of the nacelle using an UCE, a backwards interpolation with a fixed gradient can be implemented. Figure 6 compares different interpolation methods of low-resolution SCADA data. In the range from 12:47:15 to 12:47:45 it can be observed that both linear and previous value interpolation scheme differs from backwards interpolation scheme. Yaw drives rotate the nacelle constantly from 234° to 250° during this period rather than with interruptions as illustrated by other interpolation methods.

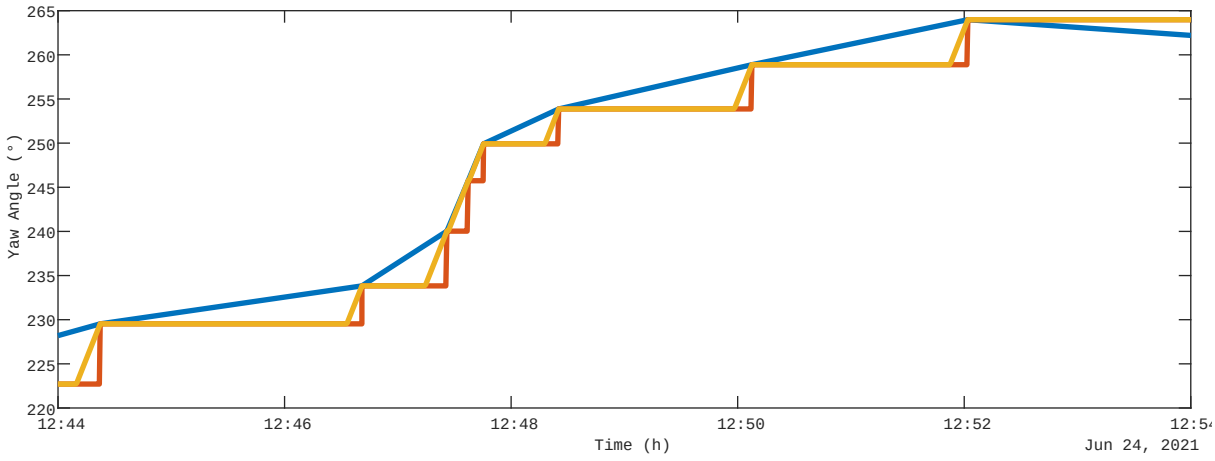


**Figure 6.** Comparison of untreated and linear interpolated yaw angle from SCADA data (blue), yaw angle using a previous value interpolation scheme (orange) and the developed backwards interpolation scheme with fixed gradient (yellow).

Due to tower bending mode shapes, accelerometer positions are influenced by tilt over time. The influence of tilt is given by $sin(\alpha)$ and is added to the respective horizontal axis. The compensation of these external influences by the respective sensor data alone is a challenging

task. Using the Z-axis of the sensor, which represents the vertical axis, the tilt of the sensor can be corrected only to a limited extent, since the change of the z-axis value due to the tilt angle is small $(1 - cos(\alpha))$ and is superimposed by noise. The ratio of the deviations in x/y and z direction is described by $\frac{sin(\alpha)}{1-cos(\alpha)}$. Figure 7 shows both normalized deviations and the resulting ratio. A tilt angle of 0.5° results in a deviation ratio of 229.2. This ratio, being large for small angles, and the superposition by noise do not allow correction of the sensor data by using the corresponding z-axis. Supplementing the influenced acceleration measurement with an inclination sensor, RTK or even both can significantly improve the acceleration and thus calculated displacement results.

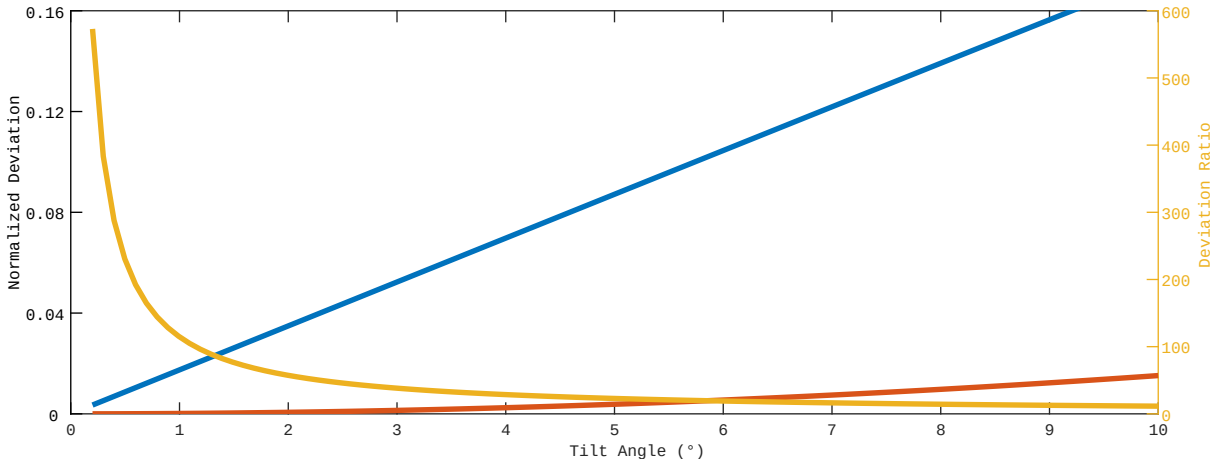


**Figure 7.** Resulting normalized deviations of x-y-axis (blue), z-axis (orange) due to tilt angle and resulting deviation ratio (yellow).

Furthermore, parametrization of the model developed in section 3.3 for mass induced strain determination is only as precise as wind influences can be excluded. Due to the applied curve fitting algorithm, short wind gusts only have a negligible influence. However, a constant wind has an effect on the parameter and particularly on $d$, i.e., the sensor offset, and thus influences the absolute calculated values. The number of usable UCEs is noticeably reduced by the fact that rotating winds triggering such an event are often associated with high air flow rates.

## 4. Simulation Model

The simulation model is achieved by first constructing a CAD model using linear geometrical entities for the simple representation of the tower geometry. Moreover, a Finite Element (FE) model is generated out of the prepared CAD model. The FE model contains cable elements that represent the tendons and beam elements for the modeling of the concrete and steel sections. In particular, one element per concrete and steel section is used. In addition, in order to represent the mass properties accurately, the material density at certain regions is adjusted, such as adapter piece, between the concrete and steel shaft as well as the rotor connection. This model serves as a simplification to the more detailed model that is created using shell and volume elements. The elasticity moduli of the individual reinforced concrete sections are determined by making use of the measured concrete dynamic elasticity modulus [12] and the rule of mixtures [13] in order to achieve a realistic material behavior and incorporate the effect of reinforcement steel.

**Table 1.** Trend of the first bending Eigenfrequency over fatigue lifetime ($n$) as a function of $S_{c,max} = [0.9, 0.5, 0.1]$ and $S_0 = 100\%$.

| n | 0.00 | 0.25 | 0.50 | 0.75 | 1.00 |
|---|---|---|---|---|---|
| $f_{S_{c,max}=0.9}$ | 0.27477 | 0.27473 | 0.27416 | 0.27165 | 0.26452 |
| $f_{S_{c,max}=0.5}$ | 0.27477 | 0.27477 | 0.27476 | 0.27390 | 0.20714 |
| $f_{S_{c,max}=0.1}$ | 0.27477 | 0.27477 | 0.27477 | 0.27468 | 0.07748 |

A particular detail of the Eigenfrequency analysis is the incorporation of the prestresses that occur due to initial displacements that are resultants of self-weight and prestressing tendons. This can be achieved by computing the equilibrium state of the structure under the loading conditions and making use of the stiffness properties at the equilibrium state. The investigations on the initial displacement effects is investigated by Wüchner et al. in [14].

## 5. Failure Cases

Simulation of the two failure cases missing prestress of tendons *(case 1)* and degradation of reinforced concrete *(case 2)* is expected to result in a direction-dependent change in stiffness and damping of the whole structure. Eigenfrequencies, nodes and antinodes are expected to vary under new conditions.

A simulation with a real load spectrum is performed. The impact on the tower is recorded by measurement. The model is optimized by means of virtual sensors. After adjusting the parameters, simulation is carried out with manipulation of the tower to generate data of a damage case by means of virtual sensors.

Making use of the FE model, a selection of degradation and failure cases are considered and the eigenfrequencies of the tower structure are computed. The considered concrete material degradation cases can be listed as follows; relative fatigue lifetime $n = [0.25, 0.5, 0.75, 1.0]$, fatigue related maximum compressive stresses $S_{c,max} = [0.9, 0.5, 0.1]$. The effect of $n$ as well as $S_{c,max}$ on the concrete elasticity modulus can be calculated using the relations from 3 [15].

$$\begin{aligned} E_c(n) &= E_{c28} * (1 - D_c(n)) \\ D_c(n) &= n^{a_c} * (1 - S_{c,max}) \\ a_c &= 26.5 - 25.0 * S_{c,max} \end{aligned} \tag{3}$$

where $E_c(n)$ is the elasticity modulus of the concrete at relative fatigue life time $n$, $D_c(n)$ is the concrete degradation coefficient and $a_c$ is the exponent factor . In addition to the material degradation, the relaxation of the prestressing tendons are considered for four different cases; $S_0 = [100\%, 95\%, 90\%, 85\%]$. Table 1 shows that the initial bending eigenfrequency changes significantly towards the end of the service life. The effect is further intensified as $S_{c,max}$ decreases.

## 6. Conclusion

The enhanced sensor configuration can be used to determine natural frequencies by means of operational modal analysis, to determine stress states in real time and provides knowledge of direction dependent condition data of the whole structure and is thus qualified to perform a comprehensive condition monitoring for supporting structures of wind turbines.

The developed processing workflow provides direct simulation input on two different ways. On the one hand, the input can be provided by calculated static and dynamic forces at the

tower top, on the other hand, the direct input can be provided by calculated displacements. The simulation input can thus be generated based on two different measurement techniques. Comparison of both inputs serves as a validation of calculations, leads to a reconciliation of both methods and enables the continuous improvement of the techniques. Operational modal analysis revealed, that acceleration based eigenfrequencies and thrust force based simulated eigenfrequencies match each other.

Comparing vibration-based displacement, processed RTK data, and simulation data with strain measurement-based external force input, the results are remarkably reproducible. The simulation was performed with the updated beam model considering only the first bending natural frequency in two spatial directions. Figure 8 shows a period of time in which the turbine was switched off at medium wind speeds of approximately 4.4 m/s$^2$ and a wind direction of 315° (NW). Both acceleration and strain data indicate that only the first bending mode is excited during this period. Since the simulation time spanned a period of only 60 s, a settling time of 6 s is excluded from the analysis. The amplitudes and phases of the three independently calculated time series in Figure 8 (a) as well as the natural frequencies of Figure 8 (b) show broad agreement, so the described procedure is accurate enough and can be used for further studies.

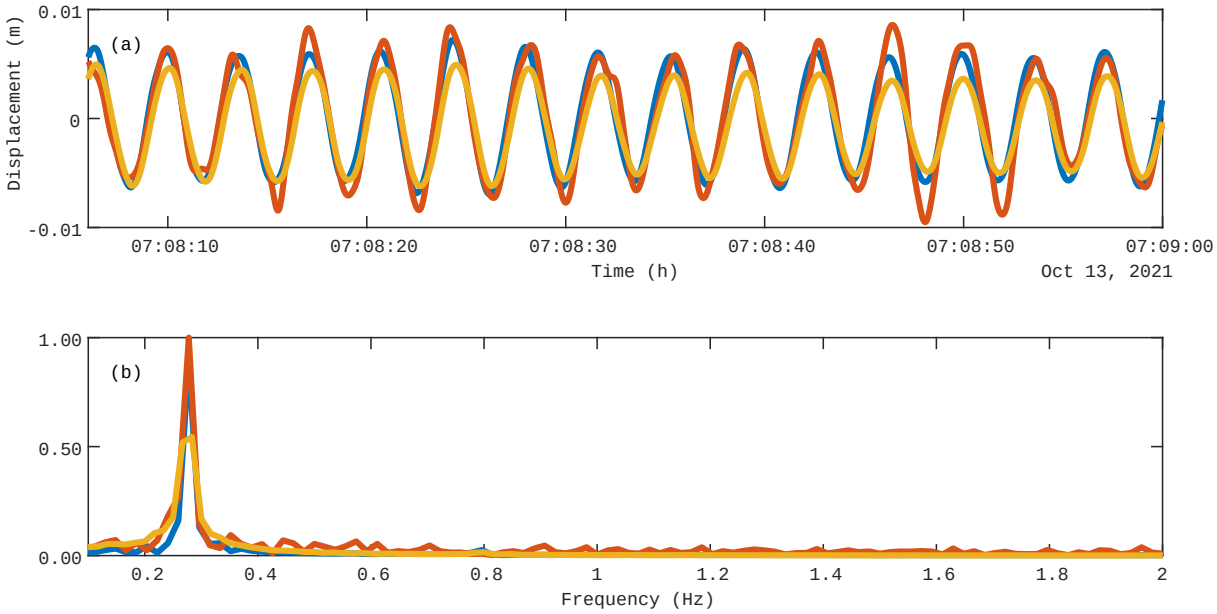


**Figure 8.** Comparison of dynamic displacement calculated using the three different approaches of vibration based displacement in frequency domain (blue), processed RTK data (orange), and external forces based simulated displacement (yellow)
(a) Comparison of time series.
(b) Normalized frequency spectra of the data sets with peaks at first bending Eigenfrequency of approximately 0.27 Hz.

Directional dependent data for stiffness, natural frequencies and damping can be used to determine pretensioning force of tendons and degradation of reinforced concrete and is able to extend regular maintenance intervals. This results in the capability to perform predictive maintenance, thus reducing downtime and increasing overall equipment effectiveness. A reduced

sensor configuration can be used in future systems of condition monitoring for wind turbines to detect further damage and fatigue as well as to determine remaining service life which is part of further investigations within the project.

**Acknowledgments**
The authors would like to thank the German Federal Ministry for Economic Affairs and Energy for funding the project and Max Boegl and Siemens for providing access to the test facility and graduate student Alejandro Ramírez Piñero for data treatment and assistance during installation. The authors also gratefully thank the staff of Max Boegl for their support during installation of the measurement systems. Supported by TUM International Graduate School of Science and Engineering (IGSSE).

**References**
[1] Botz M, Emiroglu A, Osterminski K, Raith M, Wüchner R, Große C. Überwachung und Modellierung der Tragstruktur von Windenergieanlagen. Beton- und Stahlbetonbau. 2020 mar;115(5):342-54.
[2] Bellmer H. Schäden an Tragstrukturen für Windenergieanlagen. Schadenfreies Bauen. 2016.
[3] WindEnergie B. Umgang mit Schäden an Fundamenten von Windenergieanlagen. BWE Ratgeber. 2013.
[4] Musiał M, Grosel J. Determining the Young's modulus of concrete by measuring the eigenfrequencies of concrete and reinforced concrete beams. Construction and Building Materials. 2016 sep;121:44-52.
[5] Owen JS. Monitoring the Degradation of Reinforced Concrete Beams under Cyclic Loading. Key Engineering Materials. 2003 jul;245-246:307-14.
[6] Botz M, Zhang Y, Raith M, Pinkert K. Operational modal analysis of a wind turbine during installation of rotor and generator. In: 7th International Operational Modal Analysis Conference (IOMAC); 2017. .
[7] Astarloa A, Rodriguez M, Duran F, Jimenez J, Lazaro J. Synchronizing NTP Referenced SCADA Systems Interconnected by High-availability Networks. In: 2020 XXXV Conference on Design of Circuits and Integrated Systems (DCIS). IEEE; 2020. .
[8] Qihe L. Integration of Vibration Acceleration Signal Based on LabVIEW. Journal of Physics: Conference Series. 2019 nov;1345:042067.
[9] Yanli Yang DK Yanfei Zhao. Integration on acceleration signals by adjusting with envelopes. Journal of Measurements in Engineering. 2016;Vol. 4(Issue 2):p. 117-21.
[10] Jablonski A. Condition Monitoring Algorithms in MATLAB®. Springer International Publishing; 2021.
[11] E Cheynet. Converting acceleration to displacements records. Zenodo; 2020.
[12] Wondra B, Große CU, Raith M, Mayer T, Botz M. MISTRALWIND - Monitoring and inspection of structures at large wind turbines; Teilvorhaben Lehrstuhl für Zerstörungsfreie Prüfung, Arbeitspaket 4: Überwachungstopologie : Schlussbericht BMWi-Verbundprojekt : Laufzeit: 01.08.2015-31.07.2018. Report. 2018.
[13] Tam DKY, Ruan S, Gao P, Yu T. High-performance ballistic protection using polymer nanocomposites. In: Advances in Military Textiles and Personal Equipment. Elsevier; 2012. p. 213-37.
[14] Wüchner R, Osterminski K, Gehlen C, Emiroglu A, Bletzinger KU. Monitoring and inspection of structures at large wind turbines - MISTRALWIND, Teilvorhaben 5 - Lebensdauerakte Windenergieanlagentürme : Schlussbericht : Förderzeitraum 2015-2018. Report. 2019.
[15] Emiroglu A. Multiphysics simulation and CAD integrated shape optimization in fluid-structure interaction [Dissertation]. München: Technische Universität München; 2019.